Tellus (1989), *41B*, 391–412

Simulation of the Chernobyl dispersion with a 3-D hemispheric tracer model

By JANUSZ PUDYKIEWICZ, *Environment Canada, Atmospheric Environment Service, 2121 Trans Canada Highway, Dorval, Quebec, Canada H9P 1J3*

(Manuscript received 26 January 1988; in final form 5 August 1988)

ABSTRACT

A 3-dimensional (3-D) hemispheric tracer model is employed for the long-term simulation of the dispersion of the nuclear debris from the Chernobyl accident. The most important features of the model are a fully three-dimensional advection–diffusion equation and a simple diagnostic parameterization of the boundary-layer mixing, dry deposition and wet scavenging. The tracer model is driven by a series of meteorological fields derived from the hemispheric objective analysis scheme of the Canadian Meteorological Center (CMC). The accident scenario employed in the simulation was derived from the data presented at the post-accident meeting of the International Atomic Energy Agency (IAEA) in Vienna in August 1986. Verification of the model indicates good accuracy and substantial improvement compared to the preliminary experiments with a very simple 2-dimensional (2-D) hemispheric tracer model.

1. Introduction

The meteorological aspects of the Chernobyl accident have been analysed by numerous researchers interested in the problem of atmospheric dispersion (ApSimon, 1986; Persson et al., 1987; de Leeuw et al., 1987). Most of the emphasis in these works was on regional and continental scale numerical simulation of the transport of radionuclides using models of varying complexity. The work reported in the present paper is a continuation of the preliminary investigation of the Chernobyl dispersion with a two-dimensional model (Pudykiewicz, 1988). The results presented in this paper were obtained with a new tracer model featuring a fully 3-dimensional form of the advection–diffusion equation in the σ coordinate system and more extensive parameterization of the physical processes.

The new tracer model is driven by a series of fields derived from the objective analysis system. A predictive version of the model was also developed and tested for a time period of three days following the accident. Considering the fact that the hemispheric scale dispersion of the Chernobyl debris involves time scales of about one month, we deliberately excluded the predictive model results from this paper. In the following sections we will discuss the basic equations and numerical methods employed. The results of the simulation will be presented in the form of horizontal maps of the activity field.

2. The tracer model

The most general form of the equations governing the transport of atmospheric tracers is given by a set of advection equations in flux form:

$$\partial n_v^i/\partial t = -\nabla J^i + S^i(n_v^1, \ldots, n_v^M, X), \tag{1}$$

where:

n_v^i volumetric mixing ratio (particles $*$ m^{-3})
$J^i = n_v^i V + n_v^i v_g^i k$
V 3-D velocity vector
v_g^i settling velocity
k [0, 0, 1]
∇ gradient operator

S^i sum of all external sources and sinks
X vector of all external variables describing the state of the atmosphere.

In the analysis of the problems involving radioactive tracers, it is convenient to transform equation (1) to the specific activity form:

$$\partial A^i/\partial t = -V\nabla A^i - (1/\rho)\nabla k v_g^i \rho A^i + S^i(A^1, \ldots, A^M, X), \tag{2}$$

where:

A^i specific activity (Ci kg^{-1}) or (bq kg^{-1})
$A^i = \lambda^i n^i$
λ^i radioactive decay constant
n^i mass mixing ratio
S^i sum of all external sources and sinks expressed as a function of specific activities.

In our study, eq. (2) was transformed to the terrain-following coordinate system σ (Phillips, 1957). After decomposition of the variables in the resulting equations into grid cell average and fluctuating parts, followed by averaging, assuming additionally small terrain slopes and the hydrostatic approximation (Pielke, 1984) we can obtain the following equation:

$$\begin{aligned}\partial \bar{A}^i/\partial t = &-V_H^\sigma \nabla_H^\sigma \bar{A}^i - \dot{\sigma}(\partial \bar{A}^i/\partial \sigma) + v_g^i(\partial \Gamma \bar{A}^i/\partial \sigma) \\ &- \langle V_H^{\sigma'} \nabla_H^\sigma A^{i'} \rangle + \partial/\partial\sigma \Gamma^2 K_z \partial \bar{A}^i/\partial \sigma \\ &+ \bar{S}_A^i(\bar{A}^1, \ldots, \bar{A}^M, X)\end{aligned} \tag{3}$$

where:

$\bar{A}^i$ grid cell average specific activity
V_H^σ grid cell average horizontal wind vector in the σ system
∇_H^σ horizontal nabla operator in the σ system
$\dot{\sigma}$ vertical motion field in the σ system
v_g^i gravitational settling velocity
Γ $= g\sigma/RT$
g acceleration due to gravity
R specific gas constant of air
T temperature
$V_H^{\sigma'}$ fluctuation of the horizontal wind in the σ system
$A^{i'}$ fluctuation of the specific activity
$\langle\ \rangle$ averaging operator
K_z vertical diffusion coefficient
$\bar{S}_A^i$ sum of the external sources and sinks expressed as a function of the grid cell average specific activities.

The horizontal subgrid scale flux term in the σ coordinate system was left in eq. (3) in symbolic form since our knowledge of the lateral mixing in the atmosphere is not based on any rational theory. Furthermore in our numerical simulation we neglected this term completely.

Eq. (4) is solved subject to the following boundary conditions:

$$K_z \Gamma^2 \partial \bar{A}^i/\partial \sigma = \alpha^i \Gamma \bar{A}^i + \beta^i \Gamma \quad \text{for } \sigma = \sigma_B \tag{4}$$

$$K_z \Gamma^2 \partial \bar{A}^i/\partial \sigma = 0 \quad \text{for } \sigma = \sigma_T \tag{5}$$

where:

σ_B, σ_T σ at the bottom and at the top of the model domain respectively
α_i deposition velocity for the ith specie ($\alpha_i = v_d^i$), given by formulae (21)
β_i surface emission flux for the ith species.

The terms describing all internal sources and sinks have the following general form:

$$\bar{S}_A^i = Q^i - W(\bar{A}^i) + D_{ij}\bar{A}^j, \tag{6}$$

where:

Q^i source term
$W(\bar{A}^i)$ wet scavenging term
D_{ij} $M * M$ matrix describing transformation of the isotopes and radioactive decay.

The general form of the matrix D is as follows:

$$D_{ij} = \begin{vmatrix} G_1 & & 0 \\ & \ddots & \\ 0 & & G_L \end{vmatrix} \tag{7}$$

where:

L number of decay chains considered in the simulation.

The G is a two-diagonal matrix corresponding to mth decay chain:

$$G_m = \begin{vmatrix} -\lambda_1^m & & \\ \lambda_1^m - \lambda_2^m & & 0 \\ 0 & & \lambda_{k-1}^m - \lambda_k^m \end{vmatrix} \tag{8}$$

λ_i^m radioactive decay constant for ith step in the mth decay chain
k number of the steps in the decay chain.

The form of the matrix describing the coupling between isotopes enables us to consider advection and diffusion separately for each group of radionuclides belonging to the decay chain. The situation is then much simpler in comparison to the simulation of atmospheric chemistry where the analogous matrix is not sparse. In the present study the problem of the coupling between isotopes was further simplified by considering only transport of I-131 and Cs-137 belonging to the two different decay chains.

3. Numerical solution of the transport equations

The model equations were transformed to the polar stereographic projection system true at 60° N. The corresponding equations may be written as follows:

$$\partial \bar{A}^i/\partial t = (L_1 + L_2 + L_3^i + L_4^i + L_5^i)\bar{A}^i, \tag{9}$$

where:

$L_1 := -m^2 \tilde{V}_H^\sigma \nabla_H^\sigma$	horizontal advection	(10)
$L_2 := -\dot{\sigma}\,\partial/\partial\sigma$	vertical advection	(11)
$L_3^i := v_g^i\,\partial/\partial\sigma\Gamma$	gravitational settling	(12)
$L_4^i := \partial/\partial\sigma\Gamma^2 K_z\,\partial/\partial\sigma + Q^i$	vertical diffusion and source term	(13)
$L_5^i := -W(\ \ ) + D$	scavenging and decay	(14)
$\tilde{V}_H^\sigma = (1/m)\,V_H^\sigma$	wind image in the σ system	(15)
m	map scale factor	

The time discretization of (9) is performed by successively applying the operators L_1–L_5 to advance a time step Δt and then successively applying the operators in reverse order to advance a further time step. This particular method of operator splitting is described in detail in McRae et al. (1982); the "flip-flop" has the virtue of giving a second-order time truncation error, rather than the first order one that would otherwise be obtained. As noted by McRae et al. (1982), the precise choice of operator splitting is somewhat arbitrary and they chose to do it on the basis of coordinate direction, whereas we have chosen to do it on the basis of physical processes.

The horizontal and vertical advection and gravitational settling are performed using the semi-Lagrangian algorithm developed by Robert (1982) and subsequently used for pollution problems by Pudykiewicz and Staniforth (1984). The most interesting property of the above method is that a linear stability analysis shows that the time step is not limited by a Courant condition. The time step may therefore be chosen on the basis of an acceptable time truncation error (e.g., of the same magnitude as the spatial truncation error), rather than on the basis of stability considerations (which are usually far more restrictive), provided the other terms in the equations are also handled in a computationally stable manner.

The vertical diffusion is solved using the implicit method described by Concus et al. (1976). The last substep related to scavenging and radioactive decay is accomplished using the analytical solution of the following equation:

$$\partial \bar{A}^i/\partial t = L_5^i \bar{A}^i = -W(\bar{A}^i) + D_{ij}\bar{A}^j. \tag{16}$$

The area considered in the simulation performed with our new tracer model is shown in Fig. 1. The horizontal grid of the model is uniform with a resolution of 150 km on the Polar Stereographic Projection. The corresponding grid domain is 179 * 179 points centered on the North Pole.

Eleven levels were employed for numerical solution of eq. (9). Placement of the levels is shown in Table 1. The layer corresponding to $\sigma = 1$ is located at the anemometer level—z_a. The thin layer between z_a and surface is treated analytically using surface layer theory (Businger et al., 1970).

4. The meteorological input

The transport model was driven by the data stored in the archiving system of the Objective Analysis (OA) of the Canadian Meteorological Center (CMC). The OA cycle of the CMC is based on the system described by Rutherford (1977). The analysis system is executed in a 6-h cycle and uses optimum interpolation of the forecast errors in order to provide analysed wind components, geopotential, temperature and dew point depression. The driving model of the OA system is a hemispheric primitive equation spec-

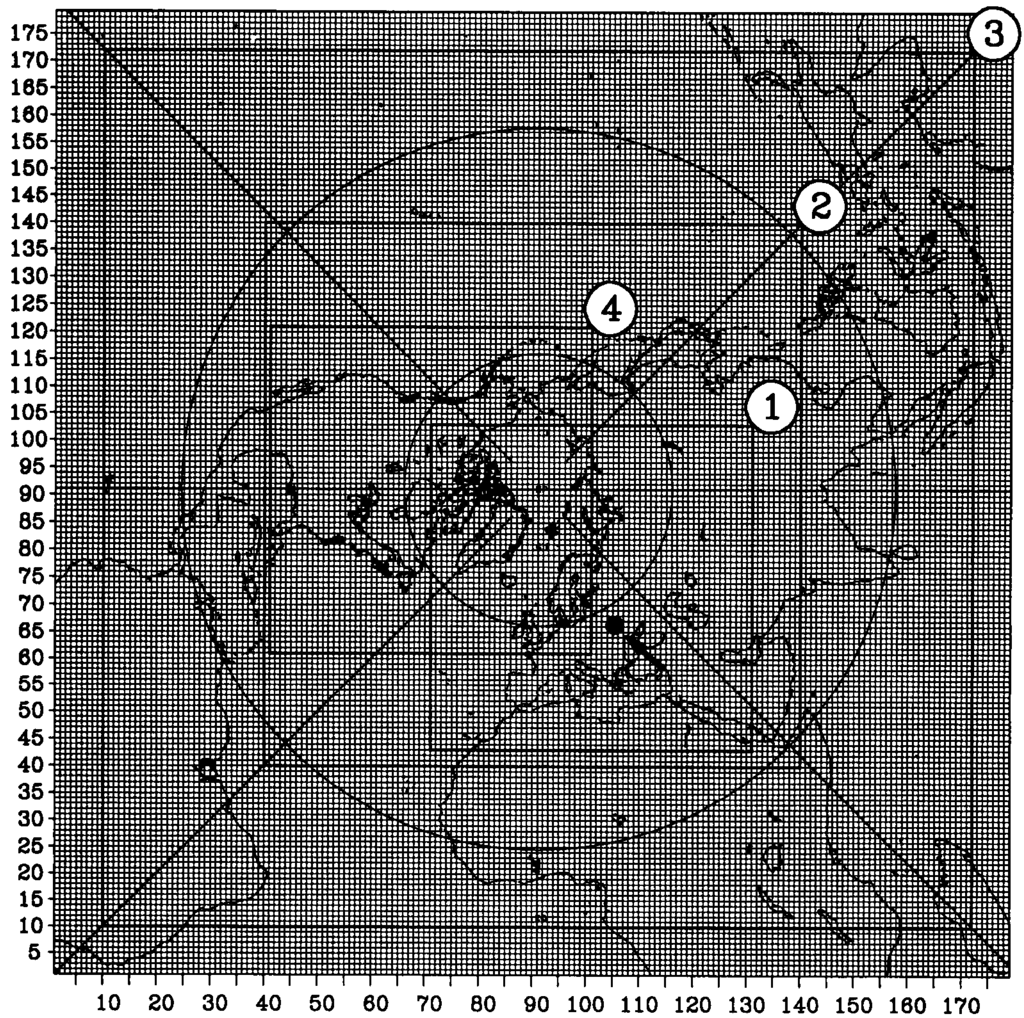

Fig. 1. The 179 × 179 horizontal mesh over which the Hemispheric Tracer Model is integrated. Windows marked: 1, 2, 3, 4 are used for display of the subsequent stages of dispersion of the radioactive cloud. The heavy dot indicated by arrow is the location of Chernobyl.

Table 1. *Placement of the vertical levels*

Level no.	σ	Level no.	σ
1	0.100	7	0.851
2	0.308	8	0.902
3	0.472	9	0.943
4	0.602	10	0.975
5	0.705	11	1.000
6	0.787		

tral model described originally by Daley et al. (1976). The function of the spectral model is to provide the 6-h forecasts required in the assimilation cycle. The forecast model is initialized using Nonlinear Normal Mode Initialization and uses a more extensive parameterization of the physical processes compared to the initial version.

The target grid of the analysis at the moment of the accident was a gaussian latitude–longitude grid with a resolution of 128 * 32 points over the Northern Hemisphere. The temporal resolution of the meteorological fields from the OA system was 6 h. The meteorological fields for intermediate time levels were obtained by time interpolation.

The vertical motion field in the σ coordinate system was obtained diagnostically from the continuity equation:

$$\dot{\sigma} = \int_{\sigma}^{1} [\mathbb{V}_{\mathrm{H}} \cdot \nabla \ln \pi + \nabla \cdot \mathbb{V}_{\mathrm{H}}] \mathrm{d}\sigma - \frac{(1-\sigma)}{(1-\sigma_{\mathrm{T}})} \int_{\sigma_{\mathrm{T}}}^{1} [\mathbb{V}_{\mathrm{H}} \cdot \nabla \ln \pi + \nabla \cdot \mathbb{V}_{\mathrm{H}}] \mathrm{d}\sigma, \quad (17)$$

where:

$\mathbb{V}_{\mathrm{H}}$ horizontal wind speed
π surface pressure
σ vertical coordinate ($\sigma = p/\pi$)
p atmospheric pressure.

This diagnostic relation is the same as the one used internally in the spectral model of the assimilation cycle and is exact in the σ-coordinate system. Its use with an analysed velocity field is debatable but entirely justified because the assimilation model of the analysis cycle undergoes an initialization step before and after each analysis step. Consequently, the wind fields are relatively free of gravity waves and the vertical motions resulting from (17) are generally acceptable for atmospheric tracer studies on the hemispheric scale over an extended time.

The profile of the vertical diffusion coefficient required to solve eq. (4) was computed externally using the analytical theory of the surface layer (Businger et al., 1970) and the O'Brien profile above the constant flux layer (Pielke, 1984):

$$K_z = K_h + \left(\frac{z-h}{H-h}\right)^2 \left\{K_h - K_H + (z-h) \times \left[\left(\frac{\partial K_z}{\partial z}\right)_h + 2\frac{K_h - K_H}{H-h}\right]\right\}, \quad (18)$$

where:

$\left(\frac{\partial K_z}{\partial z}\right)_h$ derivative of the diffusion coefficient at the top of the surface layer
h, H height of the surface layer and the planetary boundary layer respectively
K_h, K_H vertical diffusion coefficient at the top of the surface layer and at the top of PBL respectively.

The value of K_h and the profile of the diffusion coefficient in the surface layer were approximated using the relation provided by the analytical theory of the surface layer (Businger, 1971):

$$K_z = \kappa u_* z/\Phi_n(z/L), \quad (19)$$

where:

$$\Phi_n(\xi) = \begin{cases} \gamma + \alpha\xi & \text{for } \xi > 0 \\ \gamma(1-\beta'\xi)^{-1/2}; \end{cases} \quad (20)$$

ξ $= z/L$
L Monin Obukhow length
z height
κ von Karman constant
u_* friction velocity
α $= 4.7$, $\beta' = 9$, $\gamma = 0.74$.

The value of the diffusivity in the free atmosphere was assumed to be constant and equal to K_H. This approximation is sufficiently accurate for the simulation of atmospheric tracers on a hemispheric scale.

The deposition velocity appearing in the boundary condition was computed as the inverse of the sum of the resistances of the turbulent and laminar deposition layers and the resistance of the surface (Chamberlain and Chadwick, 1965):

$$v_{\mathrm{d}} = \frac{1}{r_{\mathrm{a}} + r_{\mathrm{d}} + r_{\mathrm{s}}} \quad (21)$$

where:

r_{a} aerodynamic resistance

$$r_{\mathrm{a}} = [\gamma \ln(z_{\mathrm{a}}/z_0) - \psi]/\kappa u_* \quad (22)$$

r_{d} deposition layer resistance

$$r_{\mathrm{d}} = [\gamma \ln(z_0/z_{\mathrm{d}}) + \kappa u_*/h_{\mathrm{d}}]/\kappa u_* \quad (23)$$

r_{s} surface layer resistance
ψ stability correction function
h_{d} transfer coefficient for the surface deposition layer
z_0 roughness length
z_{a} anemometer height
z_{d} height of the top of the deposition layer.

The most difficult problem in the hemispheric scale simulation of atmospheric tracers is the parameterization of wet scavenging. In general, the correct solution to this problem could be obtained only by applying a fully predictive cloud water scheme carrying explicit information about cloud and precipitating water at all model levels (Sundqvist, 1981). At this moment, the spectral model driving our assimilation cycle is not equipped with this scheme. On the other hand, the available observations of rain rates at the surface are extremely sparse and insufficient for a proper, deterministic parameterization of the wet removal in the 3-D model.

Therefore, in this study we decided to employ a very simple, statistical parameterization with a W^i term described by the following relation:

$$W^i = \begin{cases} 0 & \text{for } U < U_0 \\ \Lambda\left(\dfrac{U - U_0}{U_s - U_0}\right) & \text{for } U \geqslant U_0, \end{cases} \tag{24}$$

where:

U relative humidity
U_0 threshold value of the relative humidity above which the subgrid scale condensation occurs
U_s relative humidity for the saturation state
Λ constant.

The parameterization employed is the rain-out type and does not take into account the difference between removal by stratiform and convective clouds. The scheme given by (18) is thus restricted to large scale application over extended time intervals.

5. The source term

We approximated Q^i, the source term in our experiments with the 3-D hemispheric tracer model, by the following expression:

$$Q^i(\eta_x, \eta_y, \sigma, t) = ((E^i(t)\,F(\sigma))/(2\pi\sigma_H^2))\exp[-r^2/2\sigma_H^2], \tag{25}$$

where:

$E^i(t)$ amount of the radioactivity released
$F(\sigma)$ $= f(\sigma)\left(\dfrac{RT}{\sigma\pi}\right)\left\{\displaystyle\int_{\sigma_T}^{\sigma_B} f(\sigma)\left[\dfrac{RT}{g\sigma}\right]\mathrm{d}\sigma\right\}^{-1}$,
$f(\sigma)$ function describing vertical distribution of the release
(η_x^0, η_y^0) coordinates of the accident site
r $= ((\eta_x^0 - \eta_x)^2 + (\eta_y^0 - \eta_y)^2)^{1/2}$
σ_H standard deviation of the horizontal mass distribution ($\sigma_H = \Delta\eta_x$)
R specific gas constant of air
T temperature.

The function $E^i(t)$ was obtained from the data presented on the meeting of the IAEA in August 1986 (USSR, 1986).

The vertical distribution of the release described by the function $f(\sigma)$ was approximated as follows:

$$f(\sigma) = \begin{cases} 1 & \text{for } \sigma \geqslant \sigma_r \\ \frac{1}{2} & \text{for } \sigma_r > \sigma \geqslant \sigma_r - \Delta\sigma \\ 0 & \text{for } \sigma < \sigma_r - \Delta\sigma \end{cases} \tag{26}$$

where:

σ_r effective height of the release
$\Delta\sigma$ constant, $\Delta\sigma = 0.05$.

The σ_r was variable in our experiments, changing from 0.6, just after the explosion, to 0.8 subsequently. The effective height of the release was then between 4000 and 1500 m. The initial height of 4000 m was assumed to be in direct response to the initial explosion Pudykiewicz (1988). The smaller vertical extension, 1500, which was assumed during days following the accident represents mostly the buoyancy forces due to fire in the reactor and convective mixing in the lower part of the troposphere. The assumed vertical extension of 1500 m is in good agreement with estimates of Persson et al. (1987). The distributed source term given by relation (19) is a sufficiently good approximation for the hemispheric tracer study as indicated by our initial experiments (Pudykiewicz, 1988). For regional scale applications, the approximation involving marker particles as described by Lange (1978) would offer a more accurate alternative.

6. Results of the simulation

The hemispheric tracer model was executed for a time period of 4 weeks starting on 25 April 1986. The parameters of the run are summarized in Table 2.

During the first two days after the Chernobyl accident the radioactive cloud was transported mostly towards Scandinavia. A second southern segment of the cloud had spread south-east over

Table 2. *Parameters of the experiment*

Parameter	Value
NK	11
σ_B	1.0
σ_T	0.1
Λ	$3.5 \cdot 10^{-5}\ s^{-1}$
U_0, U_s	0.8, 1.0
λ	$\ln 2/(8.05 \cdot 24 \cdot 3600)\ s^{-1}$
σ_r	0.6 to 0.8
NI, NJ	179
ΔX	$1.5 \cdot 10^5$ m
σ_H	ΔX
α	$1/\sum$ (resistances)

the Black Sea in the direction of the Middle East (Fig. 2a). The initial stage of the transport occurred in a synoptic situation dominated by a high pressure system east of the accident site and a low located in the vicinity of Iceland. Fig. 3a shows the Mean Sea Level (MSL) pressure field on 25 April 1986, 3 h before the explosion. The pressure pattern shown remained representative for the first two days of the transport.

On 28 April the synoptic situation changed and the northern part of the radioactive cloud moved southward (Fig. 2b), crossing Poland, Germany and Austria. Subsequently on 29 April, after the dissipation of the blocking high pressure system centered north-east of Chernobyl, a well developed westerly flow began to transport radioactive material across the USSR. The representative synoptic situation for the onset of this stage of the transport is shown in Fig. 3b.

The surface values of the activity of I_{131} on 29 April are depicted in Fig. 2b. It is important to note that the cyclonic circulation system related to the deep low centered in the region of Iceland began to move radioactive material from Scandinavia and the eastern part of the North Sea towards Greenland. The most important conclusion to be drawn from the analysis of the initial stage of the transport is that the two major directions of transport to the Western Hemisphere were established at the end of April 1986 (Fig. 2b).

During the following days, the radioactive cloud was transported along these two major routes towards North America. On 2 May, the radioactive cloud spread over Greenland and the region of small activities approached the northern part of Quebec (Fig. 4a). The part of the cloud travelling along the westerlies was separated from the arctic part of the cloud by the high pressure system which had developed over the North Pole (Fig. 4b). It is important to note that at this time the amount of radioactive material transferred to Greenland was still quite large

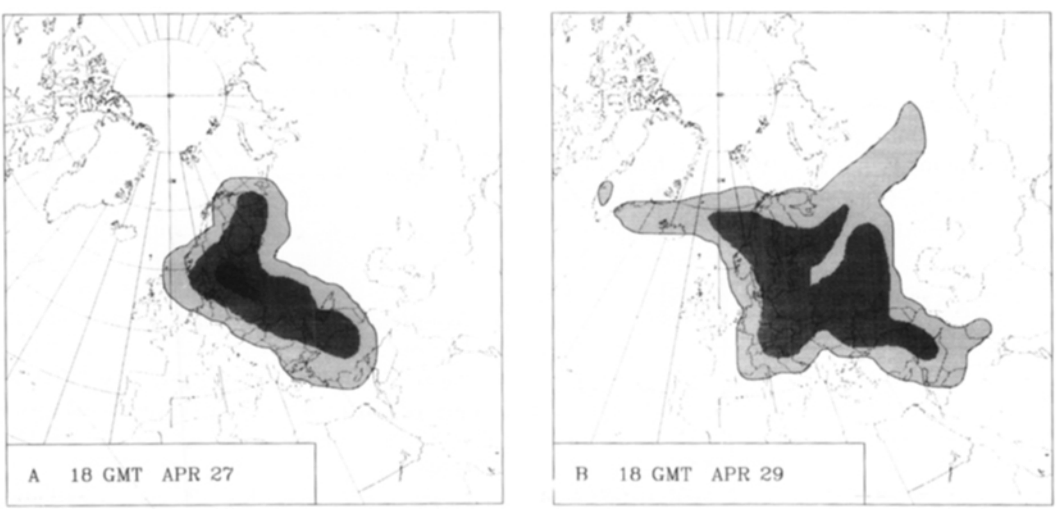

Fig. 2. Activity fields (bq kg^{-1}) for I_{131} at $\sigma = 1$ after (a) 48 h and (b) 96 h. Activities between 10^{-2} and 10^0 (bq kg^{-1}) are indicated by the dashed pattern, activities between 10^0 and 10^2 (bq kg^{-1}) by the grey pattern, activities larger than 10^2 (bq kg^{-1}) by the black pattern.

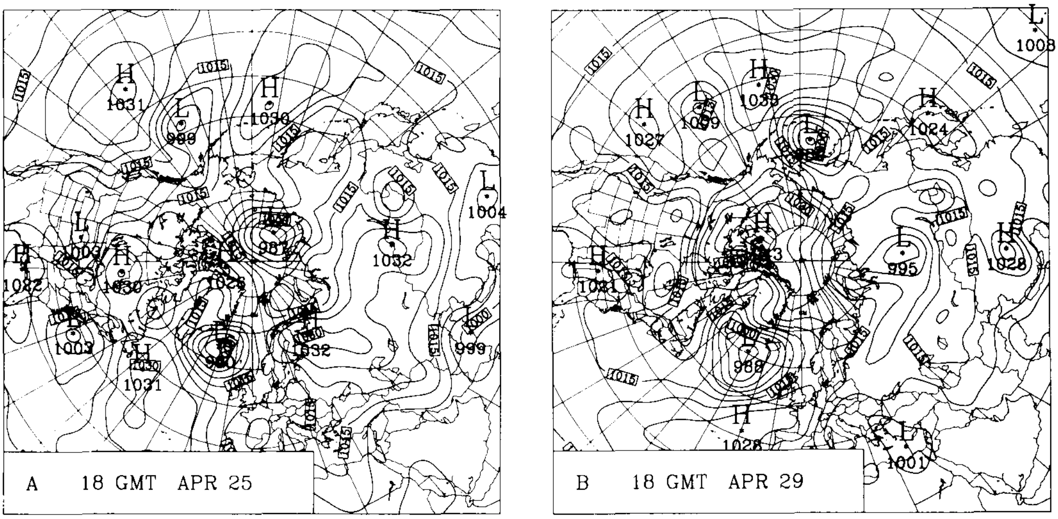

Fig. 3. Mean sea-level pressure (mb) over window 2 of Fig. 1, contour interval 5 mb, (a) for 25 April 1986, 18 GMT, (b) for 29 April 1986, 18 GMT.

despite the fact that the Icelandic low so critical to the transfer of radioactivity across the Atlantic became weaker and moved north-eastward.

On 4 May the eastern part of the cloud at the anemometer level ($\sigma = 1$) had spread across Asia and the Pacific Ocean (Fig. 5a). Note the two "spots" separated from the main body of the cloud; these are related to the descending large scale motions in high pressure system located over the eastern part of the Pacific Fig. 5b. The situation depicted in Fig. 5a is thus an example of an effect related to the 3-D character of the transport. The material travelling much faster at high levels was brought down by descending large scale motion and appeared at the surface in the region of the southern California as early as 4 May 1986. In the region of the Canadian arctic, the flow associated with the low pressure system centered over northern Quebec and the high pressure system over the North Pole transported the radioactive material westward. This transport feature is an interesting example of the easterly flow in the polar region.

On 6 May, after the dissipation of the low over Northern Quebec, the radioactive material originally spread over the arctic region moved rapidly southwestwards passing through Ontario, Quebec and the Atlantic provinces of Canada (Fig. 6c). The Atlantic part of Canada was thus affected initially by radioactive material injected from the arctic regions on 6 May. The main part of the cloud to affect the Atlantic region arrived later, namely around 8 May (Fig. 6d). The descending motions on the western side of the radioactive cloud brought down a small amount of the material from the higher levels. The radioactive material appeared along the west coast from Vancouver to Alaska and over the southwestern states of the USA.

On 8 May, the scale of the radioactive cloud became comparable to the scale of the Northern Hemisphere because eddy-like mixing by the synoptic scale low pressure systems superposed with the average zonal flow spread radioactive material towards equatorial regions (Fig. 6d). The cloud viewed on the hemispheric scale shows essentially a pattern analogous to turbulent diffusion, with low pressure systems acting as mixing eddies. The transport over Asia and Pacific was actually a superposition of the zonal flow and eddy mixing whereas transfer of the radioactive material across the Atlantic ocean had a purely eddy-like character.

The equivalent mixing process was much more rapid at the higher levels. Fig. 7 shows the position of the cloud on the hemispheric window on 2 May at the levels: 850, 700, 500 and 300 mb. The first conclusion to be drawn from Fig. 7 is that the differences between the activity field at 850 mb and at anemometer level are generally

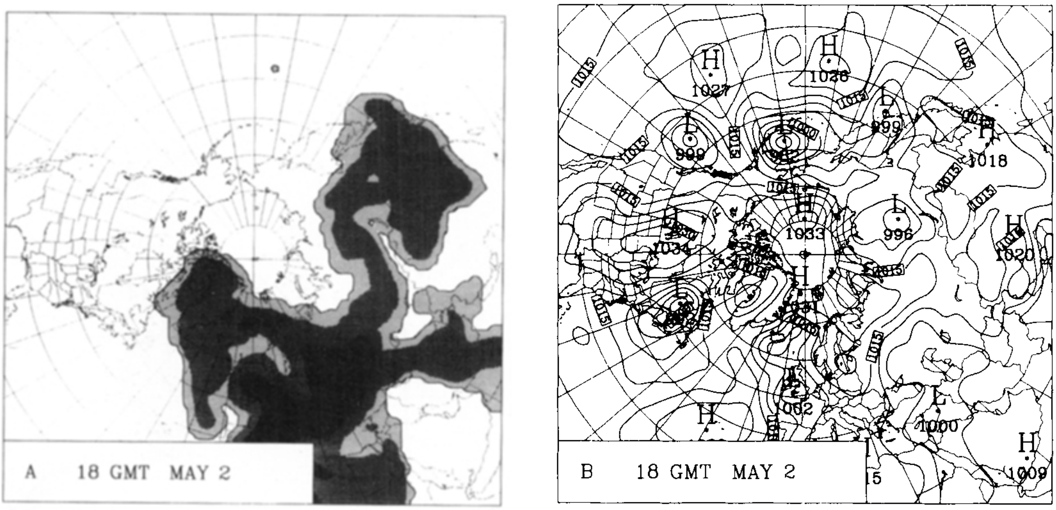

Fig. 4. Activity field of I_{131} and Mean Sea Level pressure over window 2 of Fig. 1 on 2 May 1986, 18 GMT, (a) activity field (bq kg^{-1}). Activities between 10^{-4} and 10^{-2} (bq kg^{-1}) are represented by the dashed pattern, activities between 10^{-2} and 10^{0} (bq kg^{-1}) by the grey pattern, activities larger than 10^{0} (bq kg^{-1}) by the black pattern. (b) Mean Sea-Level pressure (mb), contour interval 5 mb.

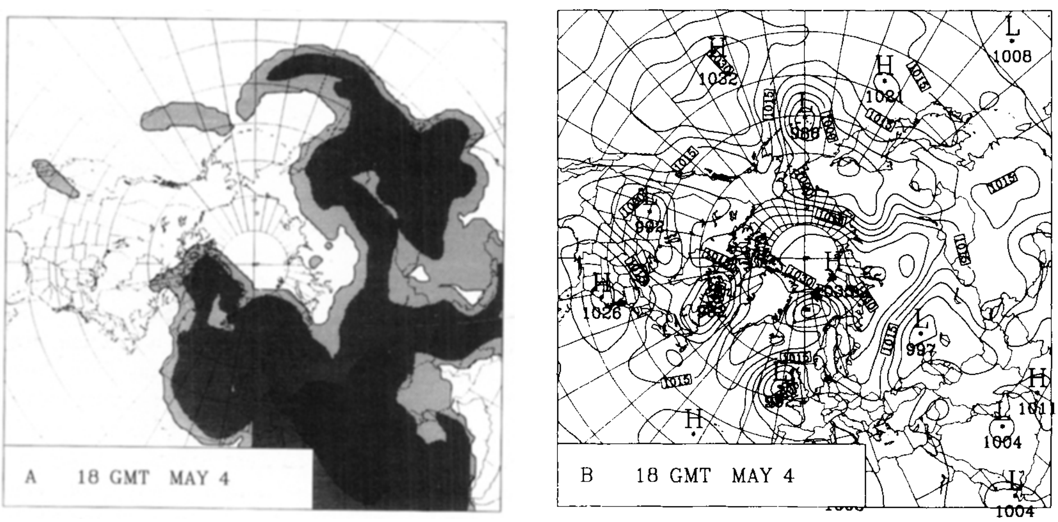

Fig. 5. Same as Fig. 4 except for 4 May, 18 GMT.

small except over the Pacific Ocean (Figs. 6a, 7a). The reason for this effect is related to boundary layer mixing and to large scale vertical motions which remove strong vertical gradients of the activity field.

The significant difference between the anemometer level activity field and higher levels is evident mostly at the 300 mb level (Fig. 7d). The most prominent feature of the high level transport is a wave-like pattern of the radioactive tracer present over the Pacific and North America. This wave-like pattern is related to the very rapid zonal transport in the jet stream of the polar front. This interesting fact is depicted separately in Fig. 8a, b, which show the tracer distribution at the 300 mb level and the 300 mb

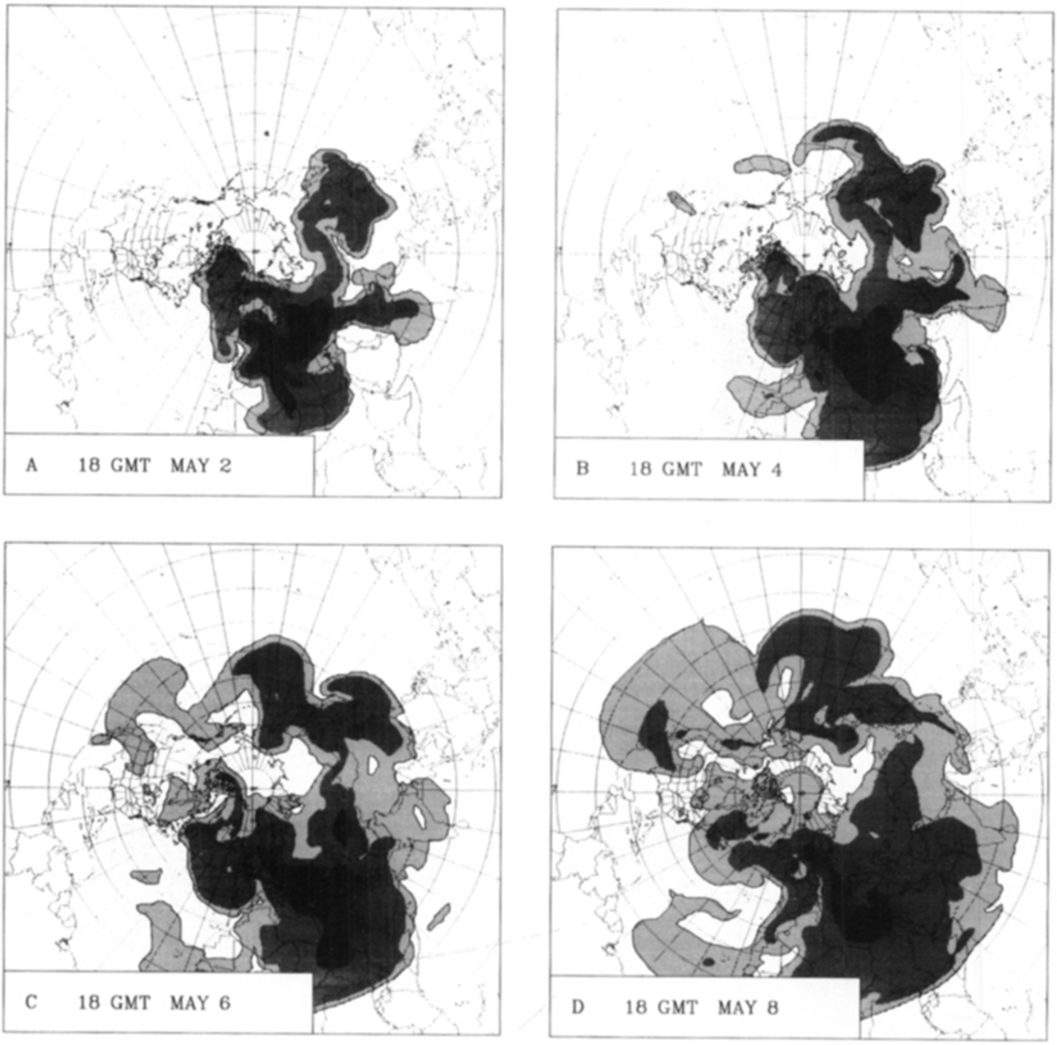

Fig. 6. Activity fields (bq kg^{-1}) for I_{131} at $\sigma = 1$ over window 3 of Fig. 1, (a) 2 May, (b) 4 May, (c) 6 May, (d) 8 May. The patterns are described in the legend of Fig. 4.

geopotential over a latitude–longitude window of our hemispheric grid. It is shown that the axis of the wave in the tracer distribution is located in the region of the maximum gradient of the geopotential height field.

7. Verification of the model

Verification of the model results was performed in this study only for the surface activities of I-131. Data for the American receptors were derived from Larsen et al. (1986) whereas the Canadian measurements were provided by Tracy (1986). The network considered in this verification study consisted of 17 stations. Experimental results to be discussed in this paper were selected to verify the most characteristic stages of the hemispheric scale transport of radionuclides from the Chernobyl nuclear accident.

Debris from Chernobyl was first detected in Finland and Sweden. According to the results of the simulation discussed in the previous chapter, radionuclides from the Chernobyl accident

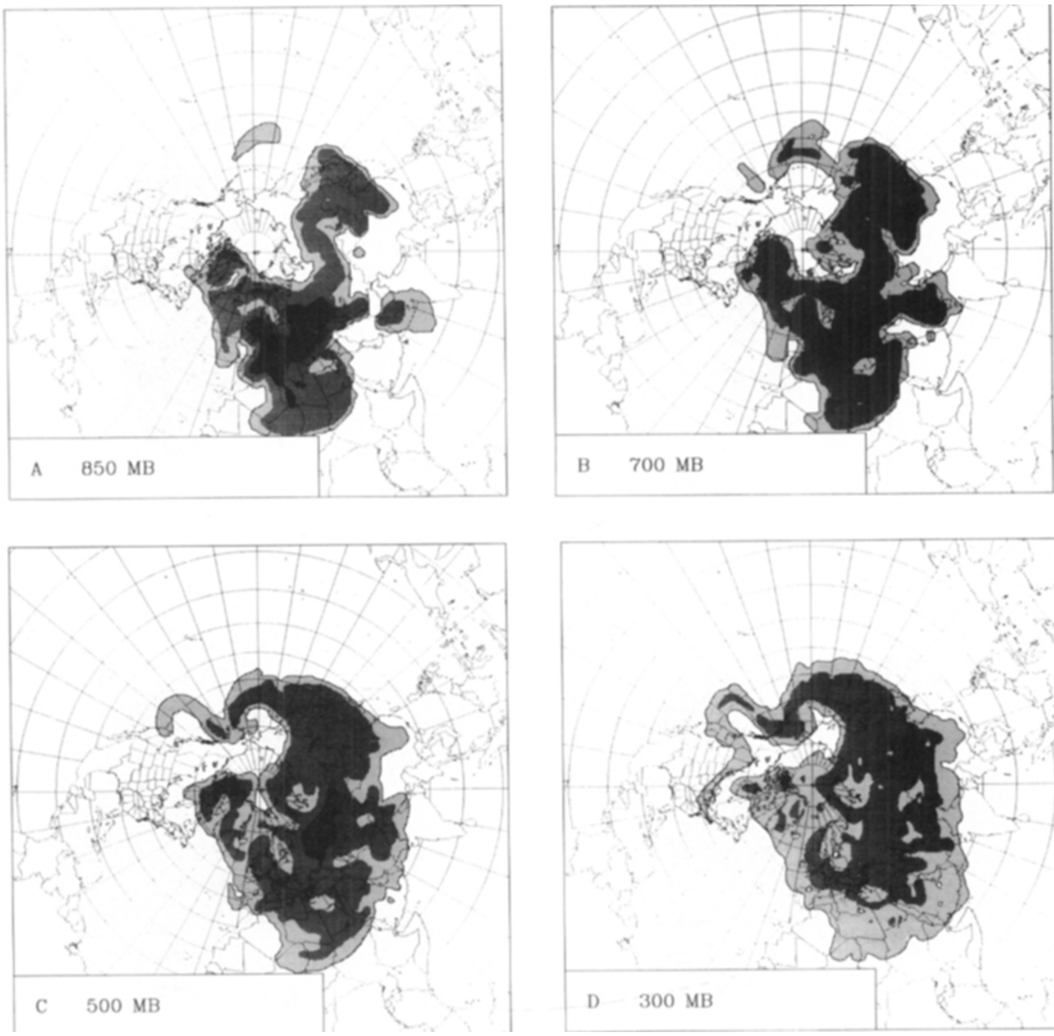

Fig. 7. Activity fields (bq kg^{-1}) for I_{131} on 2 May 1986, 18 GMT over window 3 of Fig. 1, (a) 850 mb level, (b) 700 mb, (c) 500 mb, (d) 300 mb. The patterns are described in the legend of Fig. 4.

reached Finnish air space on 27 April. Similarly, radiation levels started to rise at some of the gamma stations in Sweden on 27 April. The rising activity levels were attributed to the first cloud of contaminated air from the Chernobyl accident. The air activity from the first passage of contaminated air over Sweden reached a maximum around 29 April. Another cloud of contaminated air carrying a much smaller amount of radioactivity entered Sweden from the southeast on 9 May. The comparison of the activities of I_{131} predicted by the model at the anemometer level ($\sigma = 1$) to the values obtained from the measurements in Stockholm (Jensen and Lindhe, 1986) is shown in Fig. 9a. The model results are represented by the dashed area contained between the two lines which represent the upper and lower bounds of the model. The model bounds are defined by the following formulae:

$$f_L(t) = f_M(t) - f_\delta(t) \tag{27}$$

$$f_U(t) = f_M(t) + f_\delta(t) \tag{28}$$

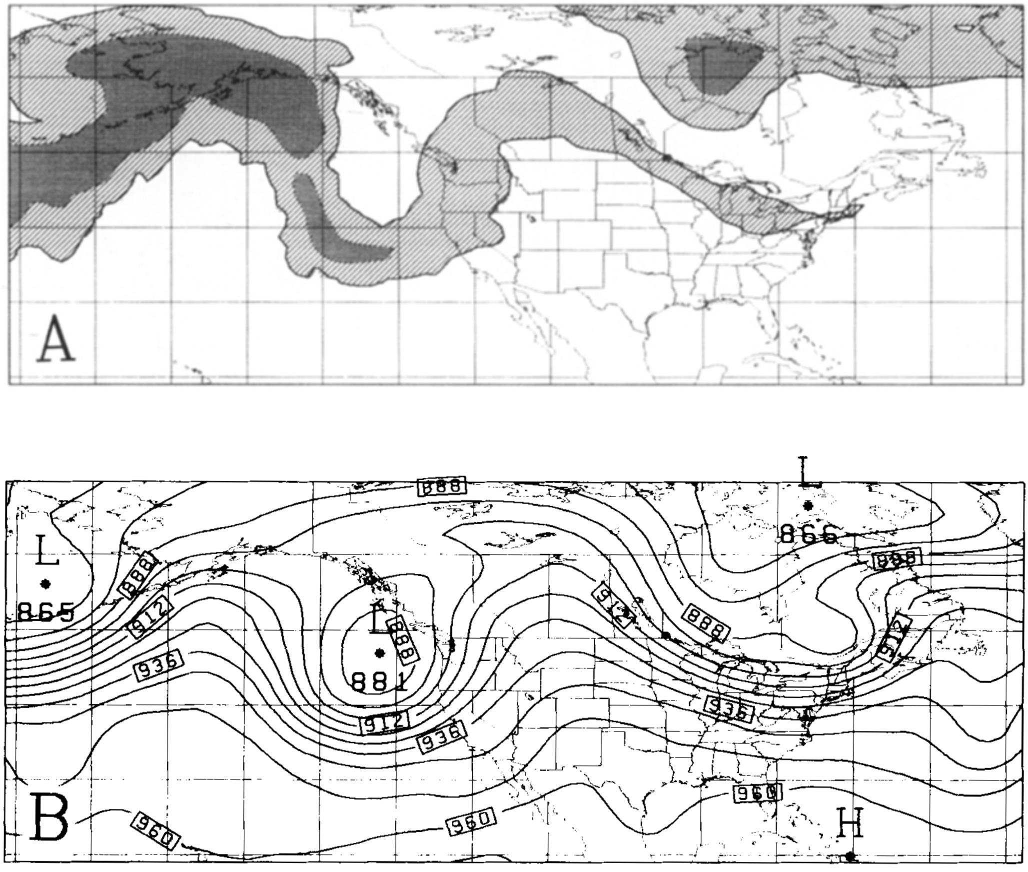

Fig. 8. (a) Same as Fig. 7d except over latitude–longitude window, (b) geopotential of 300 mb level in dkm, contour interval 8 dkm.

$$f_{\mathrm{M}}(t)=\sum_{k=1}^{n}\alpha_k f^{(k)}(t),\quad n=4 \tag{29}$$

$$f_{\delta}(t)=\left\{\left[\sum_{k=1}^{n}(f_{\mathrm{M}}(t)-f^{(k)}(t))^2\right]\Big/(n-1)\right\}^{1/2}, \tag{30}$$

where:

$f_{\mathrm{L}}(t), f_{\mathrm{U}}(t)$ lower and upper bounds of the model for a particular receptor point

$f^{(k)}(t)$ the grid point values from the corner of the grid cell containing the receptor point

α_k the weights of interpolation.

The measured values of the activity are represented by the vertical error bars. For the purpose of display, we assumed that the error is 30%, as was done in the paper describing the 2-D model results (Pudykiewicz, 1988). The analysis of Fig. 9a indicates a very good coherence between specific activities observed at the surface and simulated values at the anemometer level. The time variations of the specific activity are reproduced very well throughout the simulation. It is remarkable that the prediction of the time of arrival as well as the simulation of the second maximum of activity are very accurate.

As indicated by our simulation, the radioactive cloud moved in a southwesterly direction from Scandinavia passing initially over Poland and

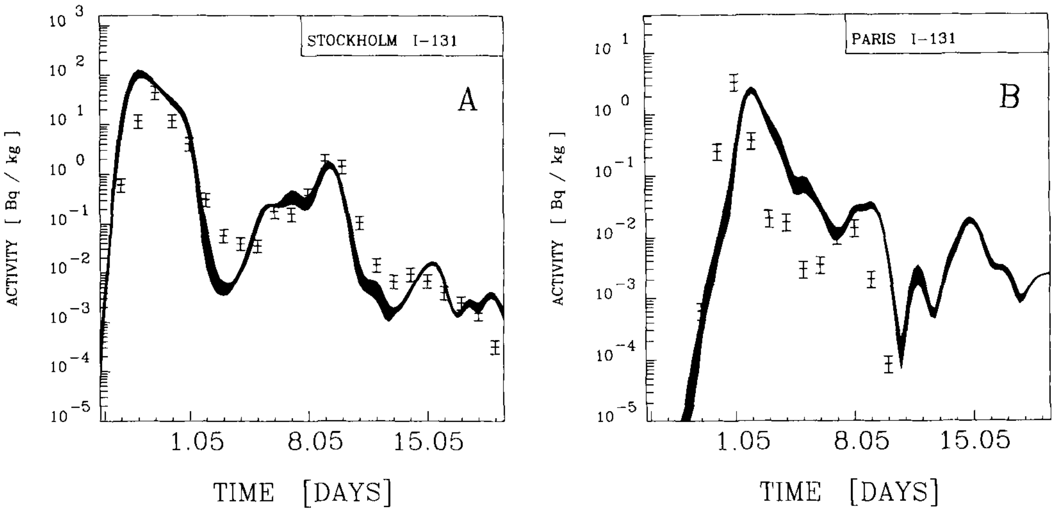

Fig. 9. Comparison of the observed and simulated time series of I-131 activity in: (a) Stockholm, (b) Paris. The measured values are represented by vertical bars, the model results correspond to the dashed area between the two lines, representing the uncertainty of the sampling process.

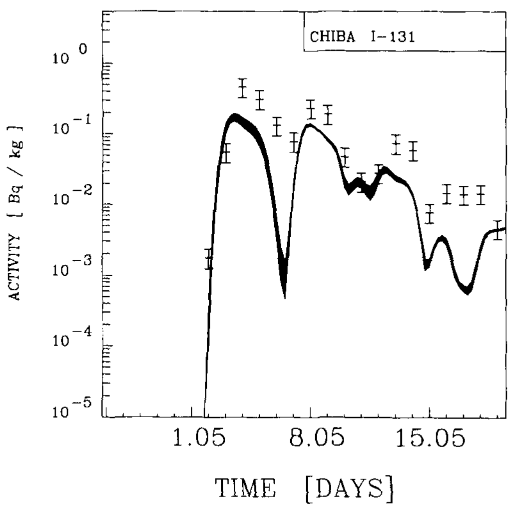

Fig. 10. Comparison of the observed and simulated time series of I-131 activity in Chiba located on Honshu Island.

finally covering Germany, Austria and Northern Italy. On 29 April the edge of the radioactive cloud at the anemometer level approached Paris. The corresponding verification of the 3-D model for Paris is shown in Fig. 9b. It is shown that the model is again very good in simulating the time of arrival of the radioactive cloud as well as the maximum activities.

Analysis of the model results indicates that the radionuclides from the Chernobyl accident transported by a steady westerly flow reached Japan on 3 May. This conclusion drawn from the numerical simulation corresponds very well to the abrupt increase of radioactivity of the surface air at Honshu Island reported by Higuchi et al. (1988). The quantitative model verification for Japan is depicted in Fig. 10 where measurements at Chiba are compared with the model results. The correspondence between the simulated and the observed times of arrival of the radionuclides is quite good. The simulation of the general trend of radioactivity at Honshu Island is also correct.

The general pattern of transfer of the radioactive material from Chernobyl to North America is depicted in Fig. 11. The results of the numerical simulation shown in Fig. 11 and discussed in the previous chapter indicate that the radioactive cloud appeared in the surface air along the West Coast of North America on 5 May. The comparison of the activities of I_{131} predicted by the model at the anemometer level ($\sigma = 1$) to the values obtained from the measurements in Rexburg (Idaho) and Vancouver (British Columbia, Canada) is shown in Fig. 12.

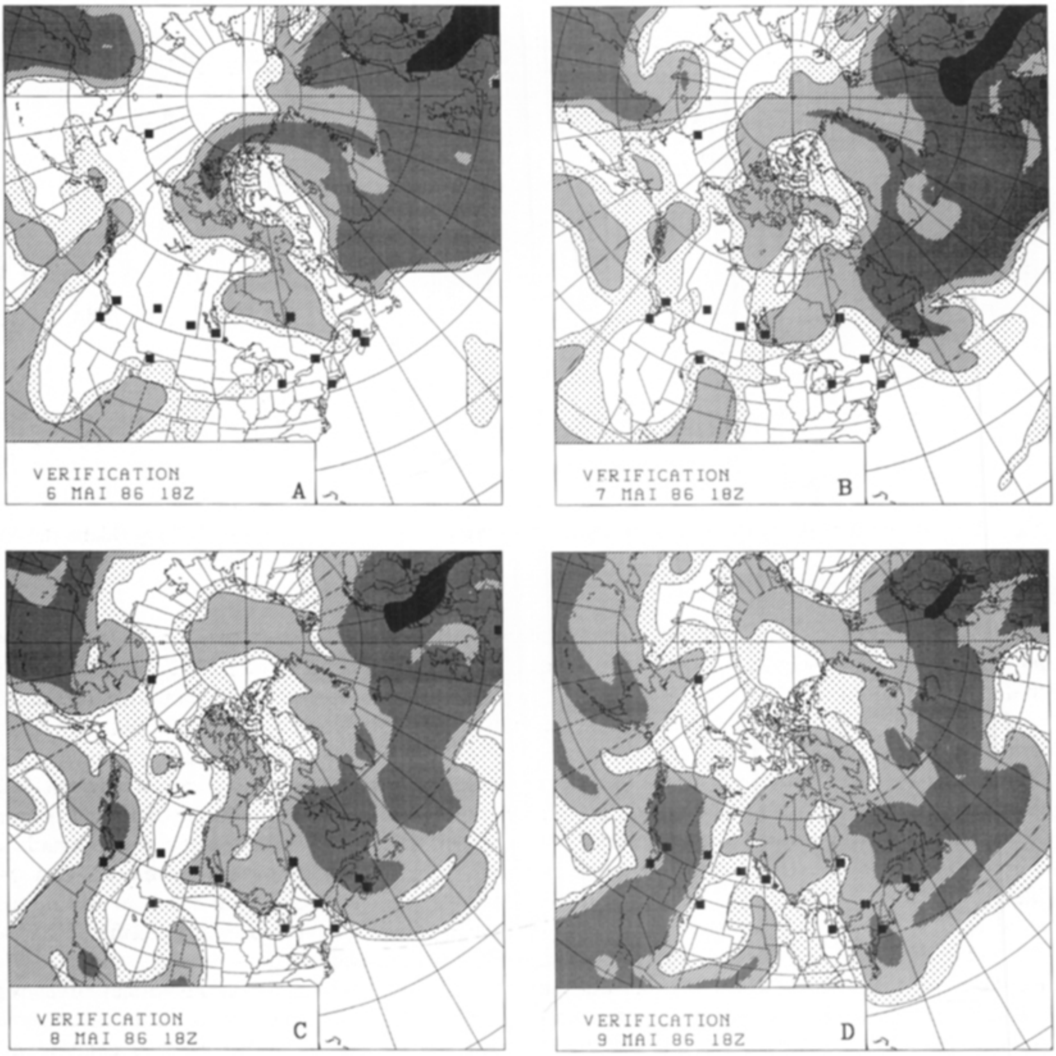

Fig. 11. Activity field (bq kg^{-1}) for I_{131} at $\sigma = 1$ over window 4 of Fig. 1, on (a) 6 May, (b) 7 May, (c) 8 May and (d) 9 May 1986, 18 GMT. Activities between 10^{-4} and 10^{-3} (bq kg^{-1}) are indicated by the dotted pattern, activities between 10^{-3} and 10^{-2} (bq kg^{-1}) by the dashed pattern, activities between 10^{-2} and 10^{0} (bq kg^{-1}) by the grey pattern, activities larger than 10^{0} (bq kg^{-1}) by the black pattern.

As before, the model results are represented by the dashed area contained between the two lines which represent the upper and lower bounds of the model. The measured values of the activity are represented by the vertical error bars. It is shown that the predicted times of arrival and time of arrival of maximum activities are reproduced by the new 3-D model with a very good accuracy.

It is important to note that the radioactive cloud affected the Atlantic and Central parts of Canada at the same time as it affected the West Coast, namely on 6, 7 May (Figs. 11a, b). The corresponding verification of the model for Moosonee (Northern Ontario), Greenwood (Nova Scotia), Winnipeg (Manitoba) and Chester (New Jersey) is shown in Fig. 13. The 3-D model is able to reproduce the effects related to the

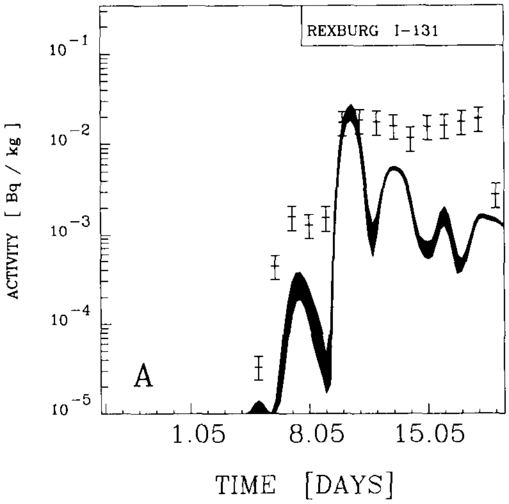

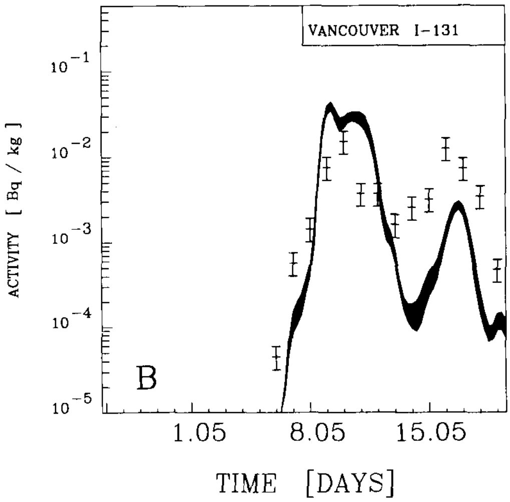

Fig. 12. Comparison of the observed and simulated time series of I-131 activity in: (a) Rexburg (Idaho, USA), (b) Vancouver (British Columbia, Canada).

initial Arctic injection of the radioactive material as well as the subsequent influence of the material transferred over the Atlantic Ocean.

In general the pattern of transfer of the radioactive material from Chernobyl to North America was quite complex. The maximum values of the activity appeared in the surface air in different locations in North America at approximately the same time, namely on 9 and 10 May (Fig. 11d). This effect can be largely attributed to the fact that the continent was affected by material travelling from across the Pacific as well as from the arctic regions and the Atlantic Ocean. The influence of material brought down from higher levels also contributed to the observed times of arrival of the maximum activity. The time series for Fredericton (New Brunswick), Ottawa, Calgary (Alberta) and Windsor (Ontario) depicted in Fig. 14 provide additional evidence of this fact.

The verification of the 3-D model for Canadian and American stations presented in Figs. 12–14 clearly indicates the good accuracy of the numerical results. It is shown that the predicted times of arrival and the times of arrival of maximum activity agree quite well with the observed values. Table 3 contains a comparison of the time average activity as simulated by the model versus time average activities obtained from observation. The ratio of the calculated and observed values varies between 0.21 and 2.80 with an average value of 1.05. Table 4 contains a comparison of the maximum activities calculated by the model to the maximum obtained from observation. The ratio of the calculated and observed maximum values varies between 0.32 and 3.22 with an average value of 1.23. The lack of perfect agreement of specific values could be attributed mostly to the large uncertainty in the specification of the source term, errors in the meteorological fields and oversimplified physical parameterizations.

The imperfections of the numerical advection scheme also have some impact on the accuracy of the tracer simulation. The series of experiments reported by Pudykiewicz et al. (1985), Ritchie (1985) and Ritchie (1987) indicate that the dispersion errors of semi-Lagrangian scheme are smaller than those for eulerian schemes. The accuracy of the simulation of the time of arrival presented in the figures is an additional indication of the accuracy of the dynamical part of our tracer model. We believe that the most important contribution to the error of our model is from the error of the analysed fields and from the error related to the parameterization of wet removal.

Statistical verification of the model is presented in Fig. 15, where results of the simulation versus measurement are compared. The horizon-

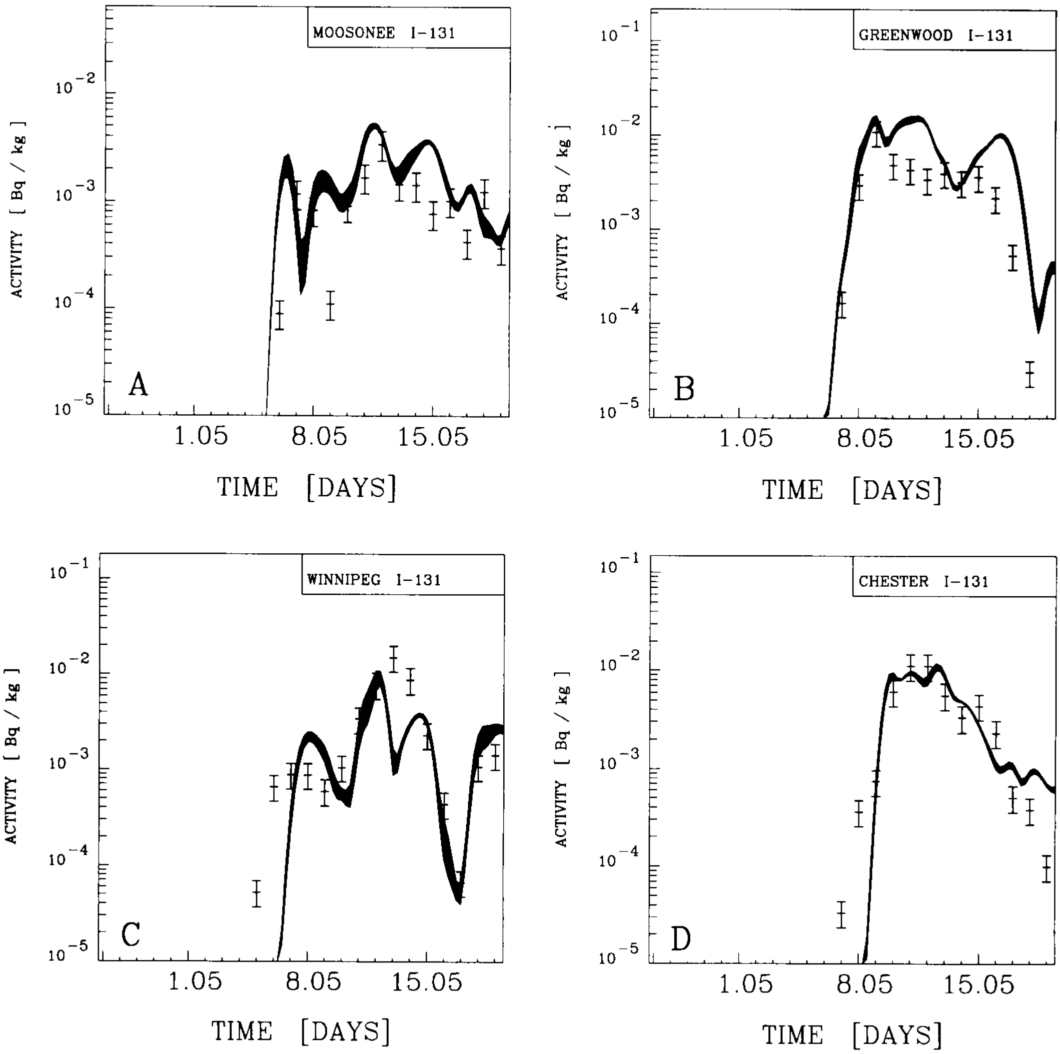

Fig. 13. Comparison of the observed and simulated time series of I-131 activity in: (a) Moosonee (Northern Ontario), (b) Greenwood (Nova Scotia), (c) Winnipeg (Manitoba) and (d) Chester (New Jersey).

tal bars are equal to the model uncertainty defined by eq. (30) and the vertical bars are equal to the arbitrary assumed error of the measurements. A diagram such as Fig. 15 is called a scatter diagram. The analysis of the scatter diagrams for the analysed receptor points indicates that in all cases the points are spread quite uniformly around the diagonal of the graphs. The coefficients of the regression line:

$$y = \alpha_2 + \beta_2 x \tag{31}$$

fitted to the experimental points on the scatter diagram using the least squares method, are described by the following formulae:

$$\beta_2 = \mu_{11}/\sigma_1^2 \tag{32}$$

$$\alpha_2 = \mu_y - \beta_2 \mu_x, \tag{33}$$

where:

$$\mu_{11} = \frac{1}{N}\left[\sum_{i=1}^{N} (x_i - \mu_x)(y_i - \mu_y)\right] \tag{34}$$

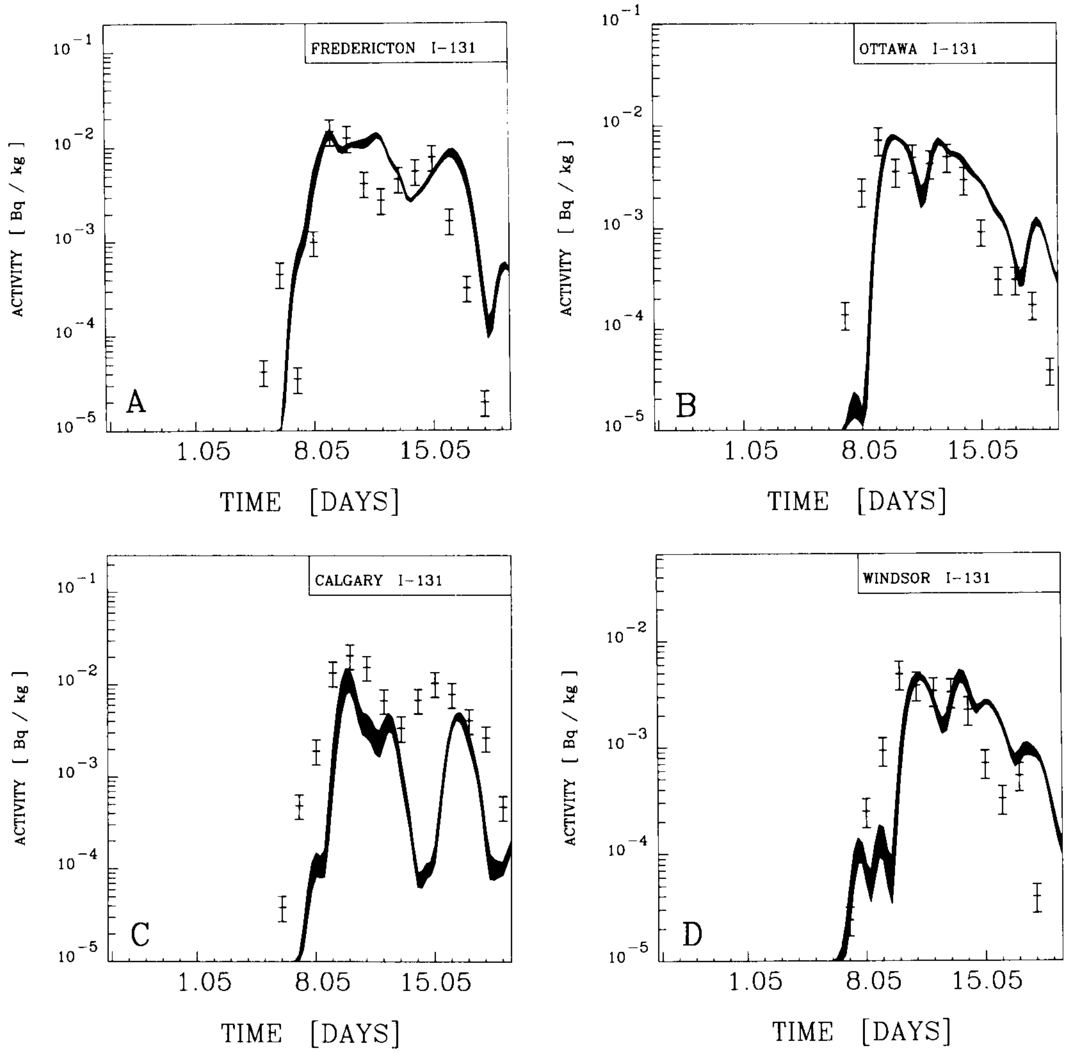

Fig. 14. Same as Fig. 13 but for (a) Fredericton (New Brunswick), (b) Ottawa, (c) Calgary and (d) Windsor (Ontario).

$$\mu_x = \frac{1}{N}\sum_{i=1}^{N} x_i, \quad \mu_y = \frac{1}{N}\sum_{i=1}^{N} y_i \tag{35}$$

$$\sigma_1^2 = \frac{1}{N}\sum_{i=1}^{N} (x_i - \mu_x)^2 \tag{36}$$

N number of points in the sample
x_i simulated activity at anemometer level ($\sigma = 1$)
y_i observed activity.

The regression line (31) could also be written as follows:

$$y - \mu_y = \beta_2(x - \mu_x). \tag{37}$$

The analogous regression line of x on y is given by:

$$x - \mu_x = \beta_1(y - \mu_y) \tag{38}$$

where:

$$\beta_1 = \mu_{11}/\sigma_2^2 \tag{39}$$

Table 3. *Average specific activities calculated by 3-D tracer model versus average observed values*

Station	Latitude	Longitude	Calculated	Observed	Ratio
Helsinki	60.25	25.00	4.592478	6.862424	0.67
Stockholm	59.50	18.00	9.135693	3.267491	2.80
Paris	49.00	2.00	0.157632	0.175589	0.90
Chiba	35.59	140.13	0.029616	0.073861	0.40
Rexburg	43.48	−111.50	0.001707	0.006766	0.25
Moosonee	51.27	−80.66	0.001058	0.000652	1.62
Fredericton	45.93	−66.79	0.003227	0.002351	1.37
Greenwood	45.00	−65.00	0.003661	0.001683	2.18
Winnipeg	49.87	−97.24	0.001156	0.001979	0.58
Vancouver	49.50	−123.00	0.004065	0.002720	1.49
Beaverton	45.32	−122.53	0.001835	0.001841	1.00
Barrow	71.10	−156.30	0.000194	0.000927	0.21
Windsor	42.29	−83.08	0.000865	0.000865	1.00
Ottawa	45.25	−75.71	0.001467	0.001353	1.08
Chester	40.48	−74.40	0.001958	0.001938	1.01
Calgary	51.10	−114.08	0.001147	0.004041	0.28
Regina	50.51	−104.47	0.001361	0.001441	0.94

Table 4. *Maximum specific activities calculated by 3-D tracer model versus maximum observed values*

Station	Calculated	Observed	Ratio
Helsinki	34.374115	108.824688	0.32
Stockholm	105.683430	45.000000	2.35
Paris	2.502741	3.493968	0.72
Chiba	0.173368	0.460075	0.38
Rexburg	0.022681	0.018654	1.22
Moosonee	0.005109	0.003419	1.49
Fredericton	0.013975	0.015250	0.92
Greenwood	0.015378	0.010931	1.41
Winnipeg	0.009231	0.013925	0.66
Vancouver	0.039870	0.015519	2.57
Beaverton	0.029619	0.009185	3.22
Barrow	0.000943	0.002068	0.46
Windsor	0.004584	0.004925	0.93
Ottawa	0.007638	0.007244	1.05
Chester	0.010784	0.011538	0.93
Calgary	0.011709	0.021125	0.55
Regina	0.018780	0.010750	1.75

$$\sigma_2^2 = \frac{1}{N} \sum_{i=1}^{N} (y_i - \mu_y)^2. \tag{40}$$

The correlation coefficient ρ defined as:

$$\rho = \mu_{11}/(\sigma_1 \sigma_2) \tag{41}$$

could be described by the following relation:

$$\rho^2 = \beta_1 \beta_2. \tag{42}$$

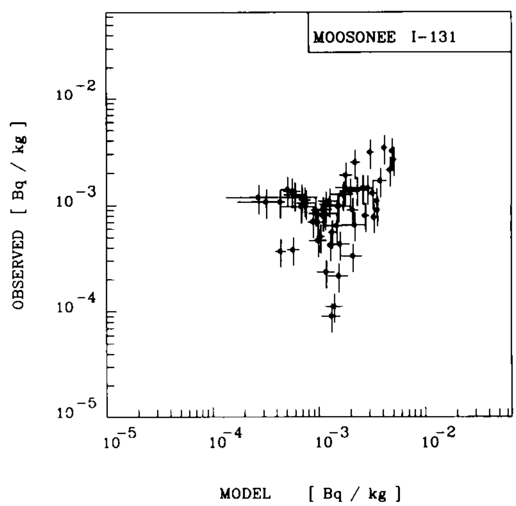

Fig. 15. Scatter diagram for Moosonee (Northern Ontario) showing simulated activities of the I-131 versus measured activities. The horizontal bars indicate the uncertainty of sampling, whereas the vertical bars represent the measurement error.

It is easy to prove that if and only if x and y are in a strict linear relationship, the two regression lines (37) and (38) coincide ($\rho = 1$). When x and y are uncorrelated the two regression lines are perpendicular. In the intermediate case, the angle between the regression lines is given by the

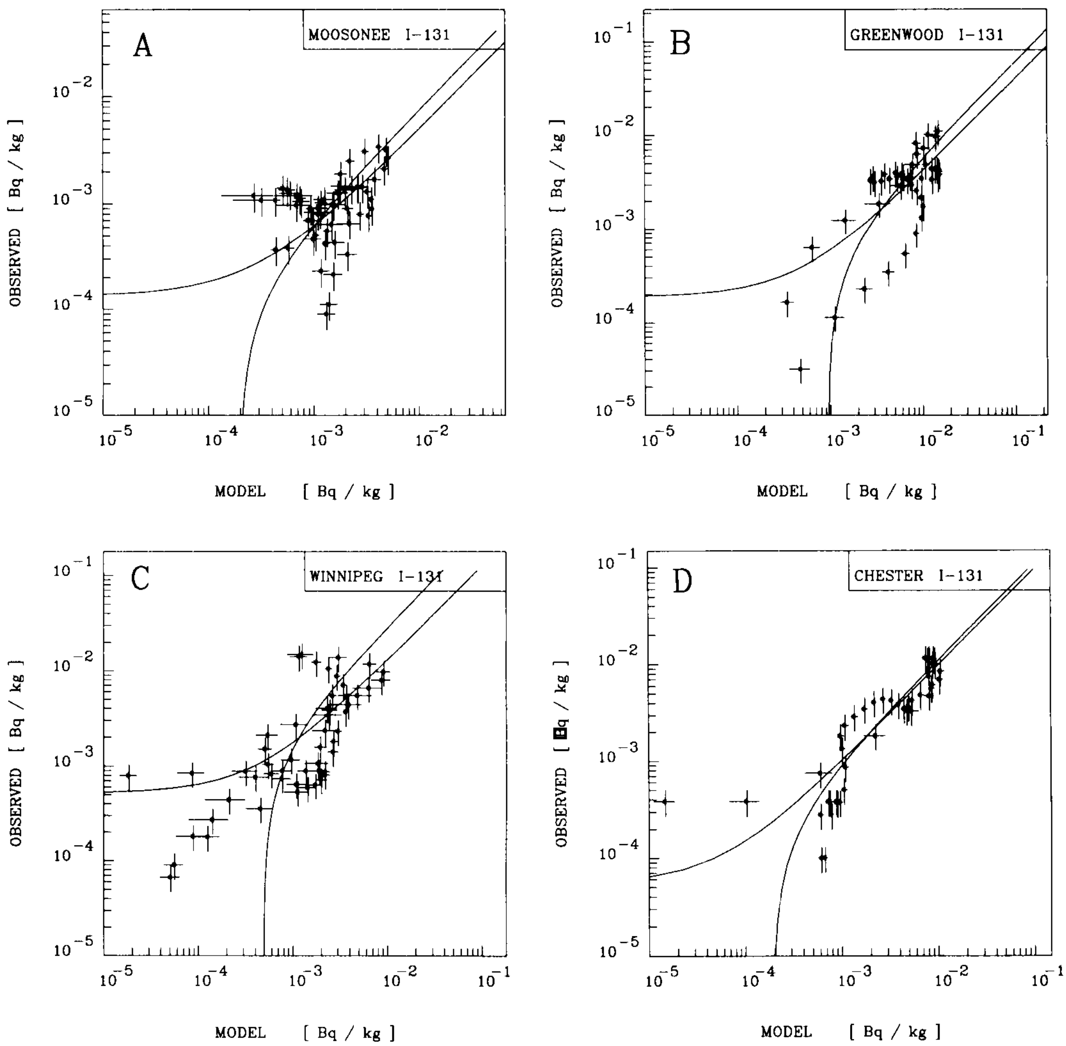

Fig. 16. The scatter diagrams and linear regression lines for (a) Moosonee (Northern Ontario), (b) Greenwood (Nova Scotia), (c) Winnipeg (Manitoba) and (d) Chester (New Jersey). Please note that the lines run almost parallel for specific activities larger than 1 mBq/kg of I-131.

following formula:

$$\vartheta = \arctan[[\sigma_1 \sigma_2/(\sigma_1^2 + \sigma_2^2)][1/\rho - \rho]]. \tag{43}$$

Table 5 contains values of the μ_x, μ_y, β_1, β_2, ϑ and ρ for the sampling points considered in our verification study. It is shown that the angle between two regression lines is always less than 1°. This indicates that the relationship between model results and observations is very nearly linear. The correlation coefficient ρ is included in Table 5 as additional information about the coherence of the simulated and observed activities. The values of ρ vary between 0.24 and 0.94 with an average value of 0.68.

Fig. 16 shows sample regression lines for four sampling points shown previously in Fig. 13. The fact that the lines are not straight is due to the use of a logarithmic coordinate system. For purposes of our discussion, it is important to note that the lines run almost parallel in the range of the

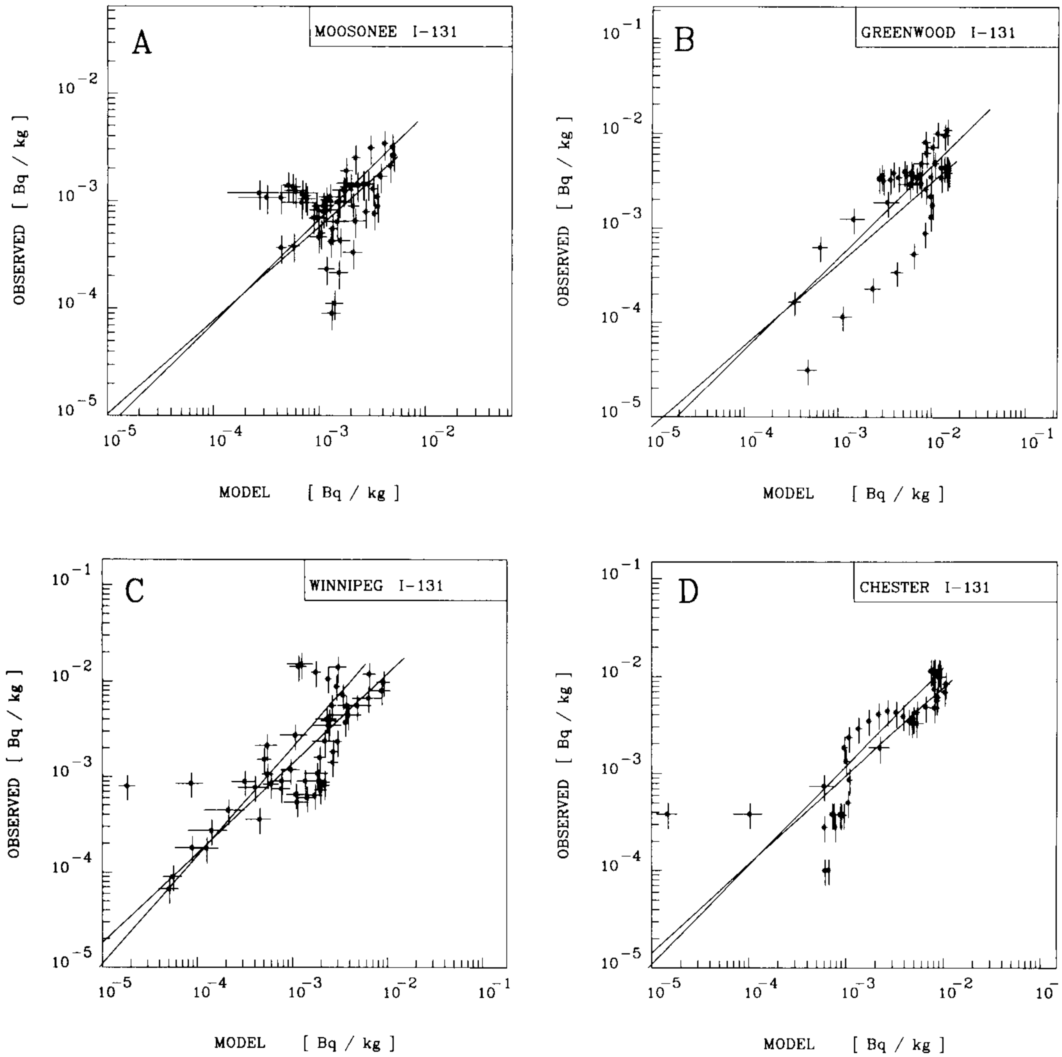

Fig. 17. Same as Fig. 16 but the regression lines were obtained from the least square fitting performed for the logarithms of the activities.

activities larger than 1 mBq/kg, which is an indication of the linear relationship between the model results and observations.

The activities considered in the hemispheric scale simulation are of the order of millions of Bequrell/kg close to the source and fractions of mBq/kg in the remote locations. Because of this extreme variability of activities the regression lines were fitted also for logarithms of the activities. This procedure allows us to examine the relation between the orders of the magnitude of the observed and simulated activities. Fig. 17 shows the results of the logarithmic least square fit for the group of receptors displayed previously in Fig. 16. The angle between two regression lines is very small which is an indication that orders of magnitude predicted by the model are related linearly to the orders of magnitude of the observations. The correlation coefficient for the logarithmic case $\rho_{\log}$ is displayed in Table 6 and the values of ρ for the linear case are listed in the second column for comparison. New values of

Table 5. *Parameters of the regression lines and correlation coefficient*

Station	β_1	β_2	ϑ	ρ
Helsinki	0.31	1.58	0.67	0.70
Stockholm	2.11	0.29	0.59	0.78
Paris	0.17	0.32	1.13	0.24
Chiba	0.35	2.02	0.63	0.85
Rexburg	0.27	1.01	0.78	0.52
Moosonee	1.32	0.49	0.74	0.80
Fredericton	0.84	0.68	0.80	0.76
Greenwood	1.62	0.41	0.69	0.81
Winnipeg	0.34	1.26	0.73	0.65
Vancouver	1.53	0.26	0.66	0.63
Beaverton	0.94	0.23	0.80	0.47
Barrow	0.09	1.61	0.59	0.38
Windsor	0.68	0.77	0.81	0.72
Ottawa	0.85	0.70	0.80	0.77
Chester	0.91	0.96	0.79	0.94
Calgary	0.32	2.00	0.62	0.80
Regina	1.17	0.52	0.76	0.78

Table 6. *Correlation coefficient computed for logarithms of the activity versus previous correlation coefficient*

Station	$\rho_{\log}$	ρ
Helsinki	0.73	0.70
Stockholm	0.80	0.78
Paris	0.73	0.24
Chiba	0.96	0.85
Rexburg	0.93	0.52
Moosonee	0.95	0.80
Fredericton	0.84	0.76
Greenwood	0.94	0.81
Winnipeg	0.91	0.65
Vancouver	0.90	0.63
Beaverton	0.91	0.47
Barrow	0.84	0.38
Windsor	0.86	0.72
Ottawa	0.88	0.77
Chester	0.95	0.94
Calgary	0.89	0.80
Regina	0.87	0.78

the correlation coefficient are between 0.73 and 0.95 with an average value of 0.88. The fact that the $\rho_{\log}$ is so large shows that the order of magnitude of the activity field predicted by the model agrees very well with observations. The agreement between the simulated and observed values is perhaps less evident, however in view of the parameters of Table 5, we can conclude that the overall performance of the model is quite satisfactory.

8. Conclusions

The most important conclusions from the simulation performed with a new 3-D tracer model are summarized as follows:

(a) radioactive material at higher levels was moved along mostly with the average zonal westerly flow;

(b) the transfer of the radioactivity across the Atlantic Ocean occurred because of eddy-like mixing by synoptic scale low pressure systems;

(c) the influence of the synoptic scale vertical motions was manifested mostly over the eastern part of the Pacific Ocean;

(d) the continent of North America was affected initially by the material injected from the arctic regions.

An analysis of the results clearly indicates that the results from the 3-D model verify better than the previous 2-D model (Pudykiewicz, 1988). The most important factor improving the hemispheric scale simulation was the incorporation of vertical motions. The presence of the vertical motion in our simulation was particularly critical for the correct simulation of the transfer of radioactive material to the west Coast of North America.

The simulation described here is a good indication that with the computing power currently available and with high resolution numerical models, it is possible to treat advection dominated processes with good accuracy. We do not suggest that the model described here will perform under other circumstances as well as it has performed on the Chernobyl case. More research related to the parameterization of mesoscale processes is needed in order to further refine the technique. The good verification of the present tracer model should increase confidence in the possibility of accurately simulating atmospheric tracers.

9. Acknowledgements

The author wants to express his gratitude to Dr. P. Merilees for his continued interest shown in this study. Discussions with Dr. C. Chouinard of RPN were very helpful to gain more insight into problems of the Objective Analysis. Thanks are also due to Mr. Bruce Brasnett of CMC who read a draft of this paper and to Dr. Clive Temperton of RPN for his careful internal review.

REFERENCES

ApSimon, H. and Wilson, J. J. 1986. Tracking the cloud from Chernobyl. *New Scientist 17*, 42–45.

Businger, J. A., Wyngaard, J. C., Izumi, Y. and Bradley, E. F. 1970. Flux-profile relationships in the atmospheric surface layer. *J. Atm. Sci. 28*, 181–189.

Chamberlain, A. C. and Chadwick, R. C. 1986. Transport of iodine from atmosphere to ground. *Tellus 18*, 226–237.

Concus, P., Golub, G. H. and O'Leary, D. P. 1976. A generalized conjugate gradient method for the numerical solution of elliptic partial differential equations. *Rep. No. STAN-CS-76-533*. Computer Sci. Dept., Stanford University.

Daley, R., Girard, C., Henderson, J. and Simmonds, I. 1976. Short-term forecasting with a multi-level spectral primitive equation model. *Atmosphere 14*, 98–134.

De Leeuw Frank, A. A. M., van Aalst, R. M. and van Dop, H. 1987. Modelling of transport and deposition over Europe of radionuclides from the Chernobyl accident. *Proc. of 16th International Technical Meeting on Air Pollution Modelling and its Applications*. Lindau, Federal Republic of Germany.

Higuchi, H., Fukatsu, H., Hashimoto, T., Nonaka, N., Yoshimizu, K., Omine, M., Takano, N. and Abe, T. 1988. Radioactivity in surface air and precipitation in Japan after the Chernobyl accident. *J. Env. Radioactivity 6*, 131–144.

Jensen, M. and Lindhe, J. C. 1986. Activities of the Swedish authorities following the fallout from the Soviet reactor accident. Report of the National Institute of Radiation Protection, Stockholm, Sweden.

Lange, R. 1978. ADPIC—A three dimensional particle-in-cell model for the dispersal of atmospheric pollutants and its comparison to regional tracer studies. *J. Appl. Meteorol. 17*, 320–329.

Larsen, R., Sanderson, C. G., Riviera, W. and Zamichielli, M. 1986. The characterization of radionuclides in North American and Hawaiian surface air and deposition following the Chernobyl accident. *US Department of Energy Report EML-460*, 331 pp.

McRae, G. J., Goodin, W. R. and Seinfeld, J. H. 1982. Numerical solution of the atmospheric diffusion equation for chemically reacting flows. *J. Comp. Phys. 45*, 1–42.

Persson, C., Rodhe, H. and De Geer, L. E. The Chernobyl accident—A meteorological analysis of how radionuclides reached and were deposited in Sweden. *Ambio 16*, 20–31.

Phillips, N. A. 1957. A coordinate system having some special advantages for numerical forecasting. *J. Meteorol. 14*, 184–185.

Pielke, A. R. 1984. *Mesoscale meteorological modeling*. London: Academic Press, 612 pp.

Pudykiewicz, J. and Staniforth, A. 1984. Some properties and comparative performance of the semi-Lagrangian method of Robert in the solution of the advection–diffusion equation. *Atmosphere-Ocean 22*, 283–308.

Pudykiewicz, J. 1988. Numerical simulation of the transport of radioactive cloud from the Chernobyl nuclear accident. *Tellus 40B*, 241–259.

Ritchie, H. 1985. Application of a semi-Lagrangian integration scheme to the moisture equation in a regional forecast model. *Mon. Wea. Rev. 113*, 424–435.

Ritchie, H. 1987. Semi-Lagrangian advection on a guassian grid. *Mon. Wea. Rev. 115*, 608–619.

Robert, A. 1982. A semi-Lagrangian and semi-implicit numerical integration scheme for the primitive meteorological equations. *J. Meteorol. Soc. Japan 60*, 319–325.

Rutherford, I. D. 1977. An operational 3-dimensional multi-variate statistical objective analysis scheme. Notes Scientifiques et Techniques, Division de Recherche en Prevision Numerique, Montreal, Canada.

Sundqvist, H. 1981. Prediction of stratiform clouds: Results from a 5-day forecast with a global model. *Tellus 33*, 242–253.

USSR State Committee. 1986. The accident at Chernobyl nuclear power plant and its consequences. Information compiled by the USSR State Committee on the utilization of atomic energy for the IAEA experts meeting, 25–29 August 1986, Vienna (available from International Atomic Energy Agency).